Mathematical Theory and Modeling
ISSN 2224-5804 (Paper) ISSN 2225-0522 (Online)
Vol.3, No.14, 2013

Numerical Investigation of the Effects of Thermo-physical Properties on Tar Intra-particle Secondary Reactions during Biomass Pyrolysis

Pious O. Okekunle*
Department of Mechanical Engineering, Ladoke Akintola University of Technology, P.M.B. 4000, Ogbomoso, Oyo state, Nigeria.

*E-mail: pookekunle@lautech.edu.ng

Abstract

In this study, a coupled transport and chemical kinetic model was used to simulate the effects of biomass thermo-physical properties on intra-particle secondary reactions during convective-radiative pyrolysis of wood cylinder ($\rho = 420$ kg/m^3) in a thermally thick regime. Wood cylinder was modeled as a one-dimensional porous solid. Solid mass conservation equations were solved by first-order Euler Implicit Method. Finite volume method was used to discretize the mass conservation equation for tar and gas, the energy conservation equation and the pressure equation. Tri-Diagonal Matrix Algorithm (TDMA) was used to solve the resulting simultaneous equations. Findings revealed that thermo-physical properties influence the extent of intra-particle secondary reactions, biomass conversion time and product yield distribution. Simulation results also showed that density has the highest influence on intra-particle secondary reactions.

Keywords: Biomass, pyrolysis, thermo-physical properties, intra-particle secondary reactions

1. Introduction

The reality of climate change engendered by the release of greenhouse gases resulting from anthropogenic activities has triggered the need for green energy sources. Biomass energy, a CO_2 neutral energy source, is considered a viable option. Aside from being CO_2 neutral, unlike fossil fuel, biomass is readily available and its supply cannot be threatened by extinction. Therefore, biomass is expected to be one of the major sources of sustainable energy in the future. In its solid form, biomass, however, is difficult to use in many applications without substantial modification. Various technologies have therefore been devised to convert and upgrade biomass into more convenient energy forms such as gaseous and liquid fuels [1]. Amongst these technologies, pyrolysis and gasification are often used [2]. In pyrolysis and gasification, tar is formed. Tar in product gases is a contaminant because it condenses, fouling process equipment and limiting the end-use of biosyngas in turbines. Therefore, one of the main challenges in pyrolysis and gasification is how to reduce tar contamination. Several methods have been used over the years for tar reduction. These include the use of scrubbers, filters, cyclone and electrostatic precipitators. The primary purpose of these devices is to capture particles from the product gas but they have also been found effective in trapping the tarry compounds present in the product gas [3]. All these methods are generally referred to as mechanism methods. Although these methods are effective, the cost involved is high and the energy content in tar is lost [3]. As a result of these short-comings, some other methods generally referred to as self-modification methods, which involve parameter modification, have been applied to reduce tar contamination in pyrolysis and gasification. In thermochemical conversion processes, parameters such as temperature, pressure, biomass type, gasifying medium and residence time are very important. The choice of these parameters can largely influence the product distribution via the degree of intra-particle secondary reactions in the decomposing solid. Many researchers have done a lot of work on the influence of temperature on tar production during biomass gasification [4-11]. Narvaez *et al.* [12] also carried out some investigations on biomass gasification at different temperatures and found that the tar content at 700 and 800 ^{o}C were 19 and 5 g/Nm^3, respectively. In our previous study, we have investigated the effect of heating rate

on intra-particle tar decomposition during pyrolysis of wood cylinder and discovered that tar decomposition increased with increase in heating rate [13]. Kosstrin [14] studied the relation between tar yield and biomass types by experimentation. It was discovered that the highest tar yield was 35% for wood, about 60% for paper and 30% for sawdust. Knight [15] carried out some investigations on biomass gasification under different pressures. Phenol was completely expunged when pressure was above 21.4 bar but Poly Aromatic Hydrocarbon (PAH) increased with enhancing pressure although total tar decreased. We have studied the effect of biomass size and aspect ratio on intra-particle tar decomposition [16]. It was discovered that tar yield decreased with increasing biomass length while the diameter was held constant. Recently, we have investigated the effect of heating rate on product yield distribution in a thermally thin regime taking into account the effect secondary reactions [17]. We found that although intra-particle secondary reactions took place, their effects were not significant due to a very short residence time. In all these studies mentioned above, there was no direct and specific investigation on the influence of biomass thermo-physical properties on tar intra-particle secondary reactions during pyrolysis or devolatilization, an important stage in gasification. Therefore this study aims at finding out the effect of thermo-physical properties on intra-particle secondary reactions.

2. Pyrolysis Mechanism

As in the previous study [17], the pyrolysis mechanism adopted was proposed by Park *et al.* [18]. As shown in Figure 1, the virgin biomass (wood) primarily decomposes by three competitive endothermic reactions to yield gas, tar and intermediate solid. The tar generated from primary pyrolysis undergoes secondary reactions yielding more gas and char. The intermediate solid, however, further decomposes through exothermic secondary reactions only into char. A detailed description of this model has been given by Park *et al.* [18]. Tar, being an extremely complex mixture, requires a huge number of chemical reactions to explain the details of its transformation during secondary reactions. It is generally difficult to account for all these reactions; hence the need to make some simplified assumptions. More explanations are given in our previous study [13].

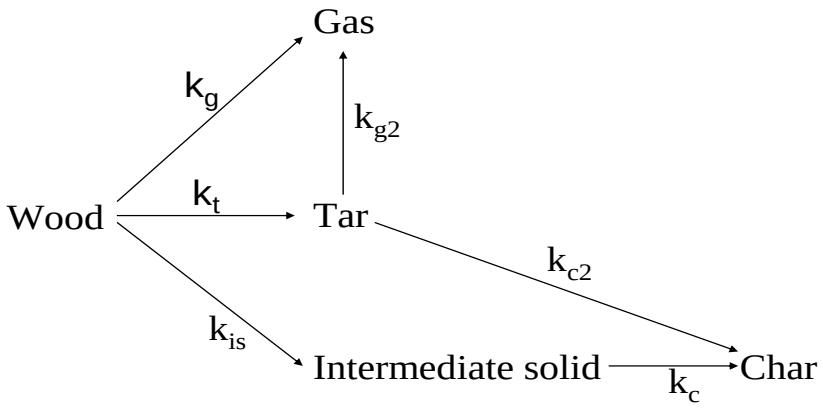

Figure1: Pyrolysis mechanism [18]

Table 2 shows the kinetic parameters used for the pyrolysis mechanism. Like other related studies, all secondary reactions by tar are considered to be exothermic [18, 19]. Reaction rates were assumed to follow Arrhenius expression of the form $k_i = A_i \exp(-E_i/RT)$. Arrhenius parameters and reaction enthalpies are as given by Park *et al.* [18]. The heats of reactions were assumed to be constant over the considered temperature range

Table 1: Kinetic parameters and heat of reaction

Reaction (i)	A_i (s^{-1})	E_i (J/mol)	Δh_i (kJ/kg)
T	1.08×10^{10}	148,000	80
G	4.38×10^{9}	152,700	80
Is	3.75×10^{6}	111,700	-300
C	1.38×10^{10}	161,000	-42
c_2	1.0×10^{5}	108,000	-42
g_2	4.28×10^{6}	108,000	-42

3. Numerical Simulation

3.1 Governing equations

The governing equations consist of the mass conservation equations and energy equation. Model assumptions in this study include the following:

- Biomass sample can be described by a one-dimensional, time dependent computational domain.

-Local thermal equilibrium exists between solid and gas phases within the particle. This presupposes that the gas leaving the particle readily heats up to the temperature of the wood char through which it flows [20].

- Components in gas phase obey ideal gas law.

- No particle shrinkage.

- Quenching of secondary reactions as soon as volatile products leave the solid surface [21].

- Diffusive transport of gaseous species within the particle pores is negligible. This implies that only mass flux by convection is considered since the effect of diffusion is very small compared to convection [20].

- Gasification reaction caused by H_2O and CO_2 released during pyrolysis is not considered. The reason for this assumption has been explained elsewhere [22].

- No condensation of tar if any migrates through the virgin solid region.

3.2 Solid mass conservation equation

The virgin biomass instantaneous mass balance equation (equation (1)) contains three competitive consumption terms, each for the reaction yielding gas, tar and intermediate solid, given as

$$\frac{\partial \rho_w}{\partial t} = -(k_g + k_t + k_{is})\rho_w \quad (1)$$

The intermediate solid instantaneous mass balance equation (equation (2)) contains two terms, one for the conversion of the intermediate solid to char and the other from tar to yield char, given as

$$\frac{\partial \rho_{is}}{\partial t} = k_{is}\rho_w - k_c\rho_{is} \quad (2)$$

Similarly, the char instantaneous mass balance equation (equation (3)) contains two terms, one for the conversion of intermediate solid to char and the other from tar transformation to char, given as

$$\frac{\partial \rho_c}{\partial t} = k_c\rho_{is} + k_{c2}\rho_t \quad (3)$$

3.3 Mass conservation equations of gas phase components

Mass conservation equations for all gas phase components are expressed by one dimensional cylindrical coordinate system consisting of both temporal and spatial gradients and source terms.

$$\text{Ar: } \frac{\partial(\varepsilon\rho_{Ar})}{\partial t} + \frac{1}{r}\frac{\partial(r\rho_{Ar}V)}{\partial r} = S_{Ar}, \quad (4)$$

$$\text{Gas: } \frac{\partial(\varepsilon\rho_g)}{\partial t} + \frac{1}{r}\frac{\partial(r\rho_g V)}{\partial r} = S_g, \quad (5)$$

$$\text{Tar: } \frac{\partial(\varepsilon\rho_t)}{\partial t} + \frac{1}{r}\frac{\partial(r\rho_t V)}{\partial r} = S_t \quad (6)$$

S_{Ar}, S_g and S_t are the source terms for the carrier gas, argon, product gas and product tar respectively and are given by:

$$S_{Ar} = 0 \quad (7)$$

$$S_g = k_g\rho_w + \varepsilon k_{g2}\rho_t \quad (8)$$

$$S_t = k_t\rho_w - \varepsilon(k_{g2} + k_{c2})\rho_t \quad (9)$$

Intra-particle tar and gas transport velocity is estimated by Darcy's law, given by

$$V = -\frac{B}{\mu}\left(\frac{\partial P}{\partial r}\right) \quad (10)$$

where μ is the kinematic viscosity. Porosity,ε, is expressed as

$$\varepsilon = 1 - \frac{\rho_{s,sum}}{\rho_{w,0}}(1 - \varepsilon_{w,0}) \quad (11)$$

where $\varepsilon_{w,0}$, $\rho_{s,sum}$ and $\rho_{w,0}$ are the initial wood porosity, the sum of solid mass density and initial wood density, respectively. The permeability B of the charring woody biomass is expressed as a linear mass interpolation between the solid phase components, given as

$$B = (1 - \eta)B_w + \eta B_c \quad (12)$$

where η is the degree of pyrolysis and is defined as

$$\eta = 1 - \frac{\rho_w + \rho_{is}}{\rho_{w,0}} \tag{13}$$

3.4 Energy conservation equation

The energy conservation equation is given as

$$\left(C_{p,w}\rho_w + C_{p,w}\rho_{is} + C_{p,c}\rho_c + \varepsilon C_{p,t}\rho_t + \varepsilon C_{p,g}\rho_g\right)\frac{\partial T}{\partial t} = \frac{1}{r}\frac{\partial}{dr}\left(r k_{eff}\frac{\partial T}{\partial r}\right) + \sum_{i=g,t,is} m_i \Delta h_i + \varepsilon \sum_{i=g2,c2} n_i \Delta h_i \tag{14}$$

where

$$m_i = A_i \exp(-E/RT)\,\rho_w \quad i = g, t, is \tag{15}$$

$$n_i = A_i \exp(-E/RT)\,\rho_t \quad i = g2, c2 \tag{16}$$

Effective thermal conductivity of the particle consists of both the conductive and radiative terms and is expressed as

$$k_{eff} = k_{cond} + k_{rad} \tag{17}$$

where k_{cond} is estimated as the weighted sum of the thermal conductivities of the virgin wood, char and volatiles, and varies with the degree of conversion. It is given by

$$k_{cond} = (1-\eta)k_w + \eta k_c + \varepsilon k_v \tag{18}$$

The radiant thermal conductivity through the pores is given by

$$k_{rad} = \frac{13.5\sigma T^3 d_{pore}}{e} \tag{19}$$

where σ, e and d_{pore} are Stefan-Boltzmann constant, emissivity and pore diameter respectively. Table 2 shows the properties of the biomass sample.

3.5 Pressure evolution

Total pressure in the process is the sum of the partial pressures of the inert gas (argon) and derived gas, given by

$$P = P_{Ar} + P_g; \;\; P_i = \frac{\rho_i RT}{M} \tag{20}$$

where M and R are the molecular weight and universal gas constant respectively. Combining equations (4), (5), (10) and (20), the pressure equation is obtained as

$$\frac{\partial}{\partial t}\left(\varepsilon\frac{P}{T}\right) - \frac{1}{r}\frac{\partial}{\partial r}\left[r\frac{BP}{\mu T}\left(\frac{\partial P}{\partial r}\right)\right] = \frac{R}{M_g}S_g \tag{21}$$

3.6 Numerical procedures

Wood cylinder was modeled as an isotropic porous solid. The pores were assumed to be filled initially with argon. As the solid was pyrolyzed, tar and gas were formed while the inert gas (argon) was released to the outer region without participating in the pyrolysis reaction. The mass conservation equations for the solid species (eqs. (1) – (3)) were solved by first order Euler Implicit Method. The mass conservation equations for gas and tar (eqs. (4) – (6)), the energy conservation equation (eq. (14)) and the pressure equation (eq.(21)) were discretized using finite volume method. Hybrid differencing scheme was adopted for the convective terms. First-order fully implicit scheme was

used for the time integral with 0.005 s time step. The computational grid number was 150. The resulting simultaneous equations were solved by Tri-Diagonal Matrix Algorithm (TDMA). Simulation converged when any of the normalized residuals of the flow parameters was less than or equal to 0.001. Figure 2 shows the computational domain and the boundary condition

Table 2: Material properties and kinetics parameters

Property	Value	Reference
$C_{p,w}$	$1500 + 1.0T$ [J/kg K]	[18]
$C_{p,c}$	$420 + 2.0T + 6.85 \times 10^{-4}T^2$ [J/kg K]	[18]
$C_{p,t}$	$-100 + 4.4T + 1.57 \times 10^{-3}T^2$ [J/kg K]	[18]
$C_{p,g}$	$770 + 0.629T - 1.91 \times 10^{-4}T^2$ [J/kg K]	[18]
d_{pore}	$5 \times 10^{-5}(1-\eta) + 1 \times 10^{-4}\eta$ [m]	[18]
σ	5.67×10^{-8} [W/m^{2}K^4]	[18]
B_w	5×10^{-16} [m^2]	[18]
B_c	1×10^{-13} [m^2]	[18]
e	0.95 [−]	[23]
h_c	8.4×10^{-3} [$W/m^2\ K^{-1}$]	[24]
μ	3.0×10^{-5} [kg/m s]	[18]
k_w	0.1046 [W/m K]	[18]
k_c	0.071 [W/m K]	[18]
k_v	0.0258 [W/m K]	[18]
$\varepsilon_{w,o}$	0.4 [−]	[18]
M_g	0.038 [kg/mol]	[18]
M_t	0.162 [kg/mol] (assumed to be levoglucosan)	
R	8.314 [J/mol K]	[18]

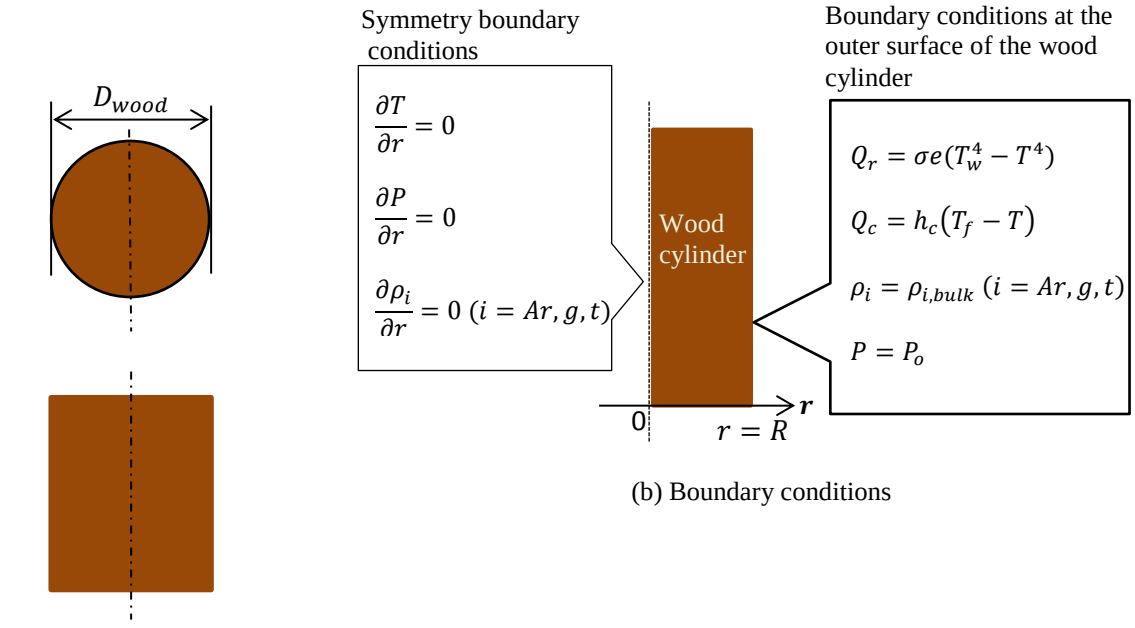

(a) Modeled wood cylinder

(b) Boundary conditions

Figure 2: Computational domain and boundary conditions

4. Results and discussion

Pyrolysis process simulations have been carried out for 30 mm diameter wood cylinders. Thermo-physical properties such as wood density, wood thermal conductivity and char thermal conductivity were varied in order to study their effects on intra-particle secondary reactions during pyrolysis. The reactor temperature was taken as 800 K (this temperature is sufficiently high for studying intra-particle secondary reactions) from the outset of the disintegration process.

4.1 Effect of biomass density

Biomass density was varied from 300 kg/m^3 to 1100 kg/m^3 in order to investigate its effect on intra-particle secondary reactions. Figure 3 shows the variation of the ratio of the rate of tar intra-particle secondary reactions (*Rs*) to the rate of primary tar formation (*Rp*) from primary pyrolysis process. The ratio *Rs/Rp* was simulated for each value of the biomass density considered. *Rp* and *Rs* were estimated as

$$Rp = \int_0^{V_c} \int_0^t k_t \rho_w dt dV_c \quad (22)$$

$$Rs = \varepsilon \int_0^{V_c} \int_0^t (k_{g2} + k_{c2}) \rho_t dt dV_c \quad (23)$$

As shown in the figure, the ratio Rs/Rp increased with increase in biomass density. This implies that the rate of tar intra-particle secondary reactions became higher while that of tar formation became lower as density increased. This will therefore lead to reduction in total tar yield and increase in gas and char yield. Figure 4 shows the temperature and velocity profiles for two different values of biomass density, which can be used to explain this result.

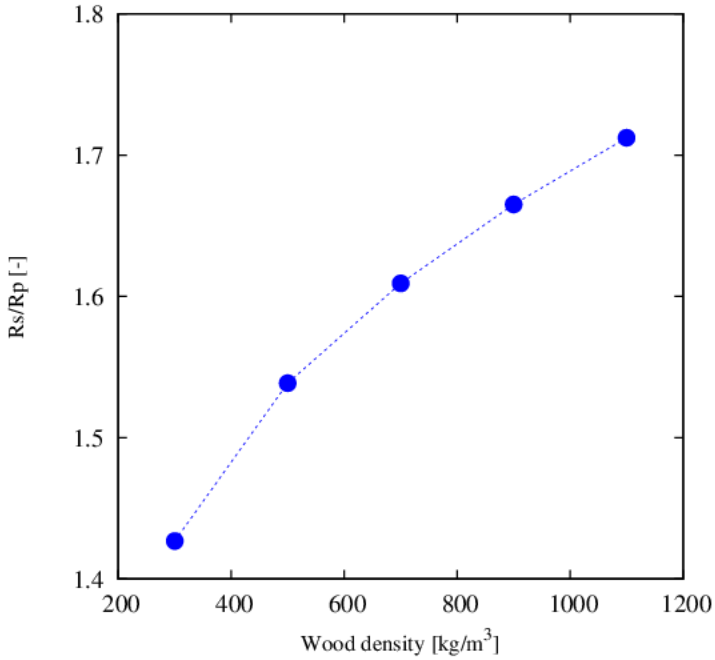

Figure 3: Effect of biomass density on Rs/Rp

As shown in Figure 4(a), as the density increased, intra-particle temperature profiles were lowered. This implies that the temperature at the primary pyrolysis front drops as the density increases resulting in slower particle heating rate. As would be expected, biomass conversion time increased with density. Residence time within the particle as density increases will therefore become longer. Figure 4(b) shows the transport velocity profiles within the particle for several elapse times at two values of density. For density of 300 kg/m^3, on the average, velocity profiles dropped with increasing elapse time. This is due to the fact that as the spatial temperature profiles increased, permeability and pores diameters also increased thereby lowering the pressure gradient, which is the driving force for the flow velocity (Eq. (10)). On the contrary, for density of 900 kg/m^3, velocity profile increased with elapse time. This is because the spatial temperature distribution, permeability and pores diameters were lower, resulting in higher pressure gradients. However, in general, velocity gradients were higher for 300 kg/m^3 than for 900 kg/m^3. Therefore, as the density increased, volatile yields from primary pyrolysis were not released in time thereby having more time to participate in the secondary reactions to yield more gas and char.

4.2 Effect of biomass thermal conductivity

In order to investigate the effect of biomass thermal conductivity, k_w, on intra-particle secondary reactions, kw was varied between 5×10^{-2} and 45×10^{-2} W m^{-1} K^{-1}. The ratio Rs/Rp was also calculated for each value of k_w. Figure 5 shows the effect of thermal conductivity on the ratio Rs/Rp. From the figure, it is seen that there was a tremendous increase in Rs/Rp from 5×10^{-2} W m^{-1} K^{-1} to 15×10^{-2} W m^{-1} K^{-1}, followed by a barely noticeable reduction in Rs/Rp from 15×10^{-2} W m^{-1} K^{-1} to 25×10^{-2} W m^{-1} K^{-1} and then a steady increase in Rs/Rp from 25×10^{-2} W m^{-1} K^{-1} to 45×10^{-2} W m^{-1} K^{-1}. Based on the foregoing, some more simulations were further carried out in order to explain these phenomena. In the first scenario i.e., tremendous increase in Rs/Rp, simulation results showed that the velocity gradients when k_w was 5×10^{-2} W m^{-1} K^{-1} were, on the average, higher than when k_w was 15×10^{-2} W m^{-1} K^{-1}. More, the temperature profiles were initially higher for 15×10^{-2} W m^{-1} K^{-1} before they

eventually approach the furnace temperature in both cases. The combination of these factors (elongated residence time within the particle and high spatial temperature distribution) enhanced better tar intra-particle secondary reactions for a thermal conductivity of 15×10^{-2} W m^{-1} K^{-1}.

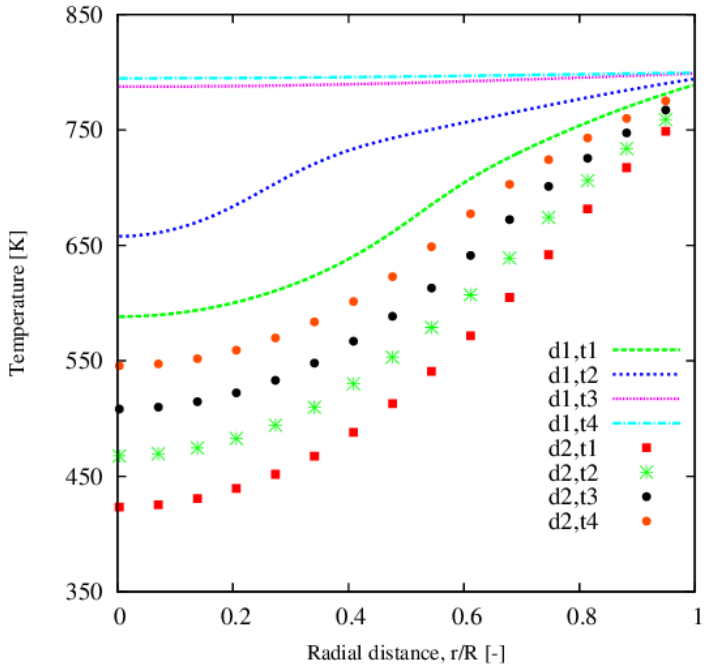

(a) Temperature profiles

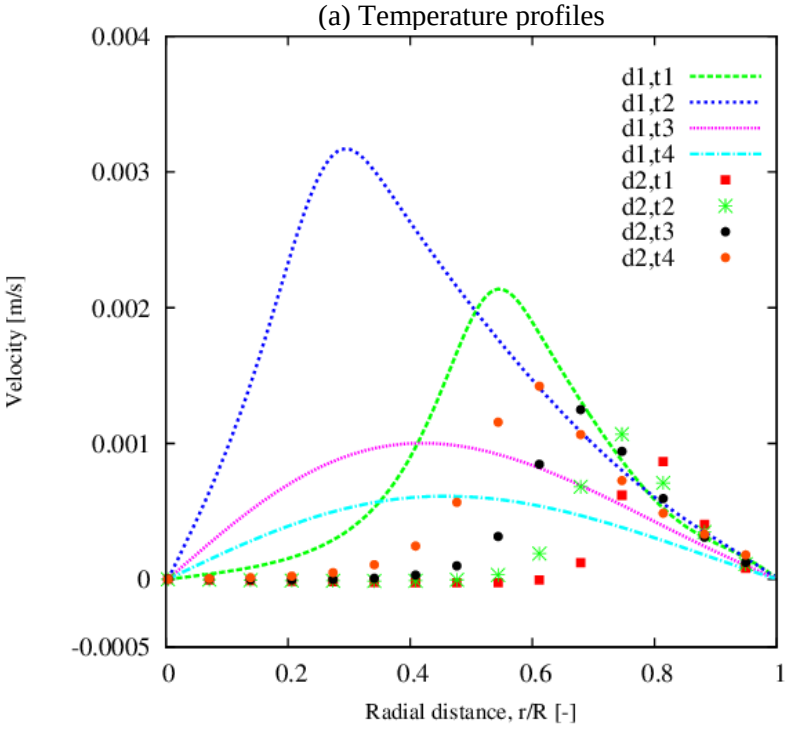

(b) Velocity profiles

Figure 4: Temperature and velocity profiles for several elapse times at two values of density: d1= 300 kg/m^3, d2 = 900 kg/m^3, t1 = 500 s, t2 = 600 s, t3 = 700 s, t4 = 800 s

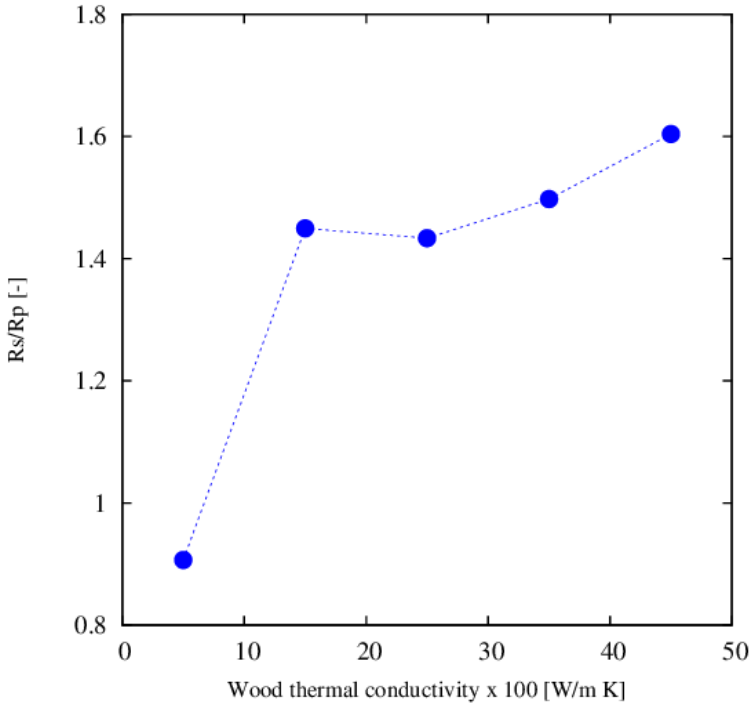

Figure 5: Effect of wood thermal conductivity on Rs/Rp

In order to explain the second scenario (a barely noticeable reduction in Rs/Rp between 15×10^{-2} and 25×10^{-2} W m^{-1} K^{-1}), some more simulations were also performed. Calculation results showed that within the first 400 s of pyrolysis, when a higher percentage of biomass conversion was accomplished, the velocity profiles were higher for 25×10^{-2} W m^{-1} K^{-1}. This implies some reduction in intra-particle residence time. Although the temperature gradients were higher initially in this case, the temperature gradients for 15×10^{-2} W m^{-1} K^{-1} leveled up after about 700 s of the process. The resultant effect was a slight reduction in the extent of tar intra-particle secondary reactions within this range. The last scenario (a steady increase in Rs/Rp between 25×10^{-2} and 45×10^{-2} W m^{-1} K^{-1}) will now be considered. Figure 6 shows the temperature and velocity gradients for two different values of biomass thermal conductivity. As shown in Figure 6 (a), as the thermal conductivity increased, temperature profiles also increased along the length of the biomass cylinder. This was because the rate of heat transfer towards the interior of the sample increased, resulting in reduction in the conversion time of the sample. The temperature gradient was however lowered with increase in thermal conductivity. Figure 6(b) shows the velocity profiles for two values of the thermal conductivity at various elapse times. As shown in the figure, the flow velocity dropped with increase in thermal conductivity and elapse time. This was because the increase in temperature profile facilitated the rate of biomass conversion, which also in turn increased the pores diameters, thereby reducing the pressure gradient that drives the fluid flow. This culminated in elongating volatile residence time within the particle. Hence, the steady rise in Rs/Rp. The overall effect of all these will most likely result in increase in gas and char yield at the expense of tar yield.

4.3 Effect of char thermal conductivity

The effect of char thermal conductivity, k_c, on intra-particle secondary reactions during pyrolysis was also investigated. The values of k_c were varied between 3×10^{-2} and 30×10^{-2} W m^{-1} K^{-1}. Figure 7 shows the effect of

char thermal conductivity on Rs/Rp. As shown in the figure, there was a barely noticeable increase in Rs/Rp from 3×10^{-2} to 8×10^{-2} W m^{-1} K^{-1} followed by a continual decrease in Rs/Rp as k_c increased. Some simulations were further performed to explain this trend. Calculation results showed that between 3×10^{-2} and 8×10^{-2} W m^{-1} K^{-1},

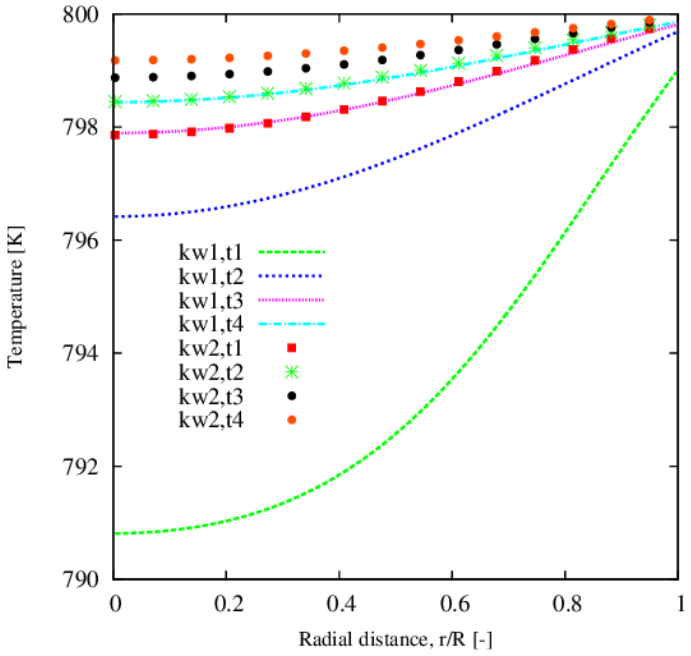

(a) Temperature profiles

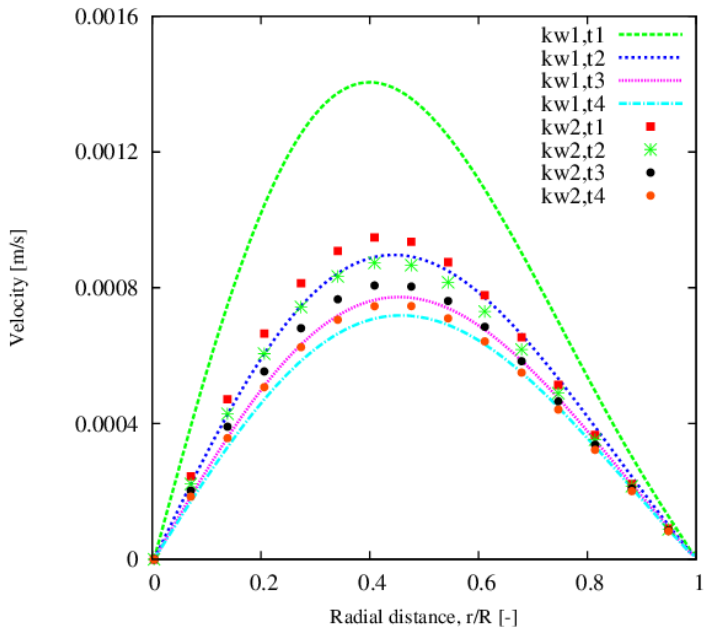

(b) Velocity profiles

Figure 6: Temperature and velocity profiles for several elapse times at two values of biomass thermal conductivity: kw1 = 15×10^{-2} W m^{-1} K^{-1}, kw2 = 25×10^{-2} W m^{-1} K^{-1} , t1 = 500 s, t2 = 600 s, t3 = 700 s, t4 = 800 s

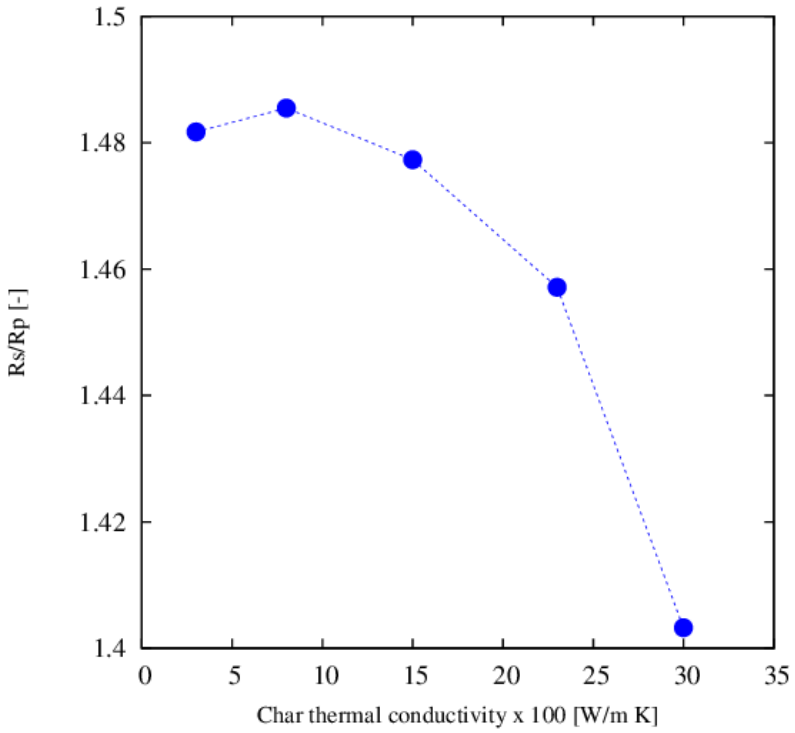

Figure 7: Effect of char thermal conductivity on Rs/Rp

within the first 400 s of the decomposition reaction, the temperature profiles for 8×10^{-2} W m^{-1} K^{-1} were a little higher than for 3×10^{-2} W m^{-1} K^{-1} while the velocity profiles were higher for the latter than the former. After 400 s, the temperature profiles for 8×10^{-2} W m^{-1} K^{-1} became much higher, approaching the furnace temperature. This however was accompanied with increase in permeability and pores diameters, thereby reducing the pressure gradient that drives the flow. The cumulative effect of all these was elongation of intra-particle residence time which favoured tar intra-particle secondary reactions. Hence, the slight increase in Rs/Rp. Furthermore, in Figure 7, some consistent reduction in Rs/Rp from 8×10^{-2} W m^{-1} K^{-1} to 30×10^{-2} W m^{-1} K^{-1} was also observed. As in other cases considered, simulations were performed to monitor intra-particle spatial temperature distribution and velocity profiles at various elapse times to explain this trend. After careful examination of the calculation results, it was revealed that the declination in Rs/Rp values with increasing char thermal conductivity from 8×10^{-2} to 30×10^{-2} W $m^{-1}K^{-1}$ will be better explained by presenting the results for the elapse time within which a higher percentage of biomass decomposition was accomplished. Figure 8 therefore shows the temperature and velocity profiles for two different values of char thermal conductivity from 100 s to 400 s elapse time. As seen in Figure 8(a), the temperature profiles gradually increased with increase in char thermal conductivity until about 300 s when there was a recognizable increase in temperature profiles. As seen, the temperature in the region closest to the surface exposed to heat increased with char thermal conductivity thereby enhancing primary pyrolysis. It implies that the rate of biomass conversion was accelerated, thereby reducing biomass conversion time. As in other cases, the temperature gradients flattened out towards the interior of the sample. Figure 8(b) shows the velocity profiles obtained for two different values of char thermal conductivity at various elapse times. From the figure, it is seen that the flow velocity increased with char thermal conductivity resulting in accelerated release of volatile yields. This shortened intra-particle residence time required for tar intra-particle secondary reactions. The combination of these events (accelerated biomass conversion rate and shortening of intra-particle residence time) will culminate in increase in tar yield as char thermal conductivity increases. It is also important to report that even after elapse time of 400 s, velocity profiles, on average, still followed the same trend.

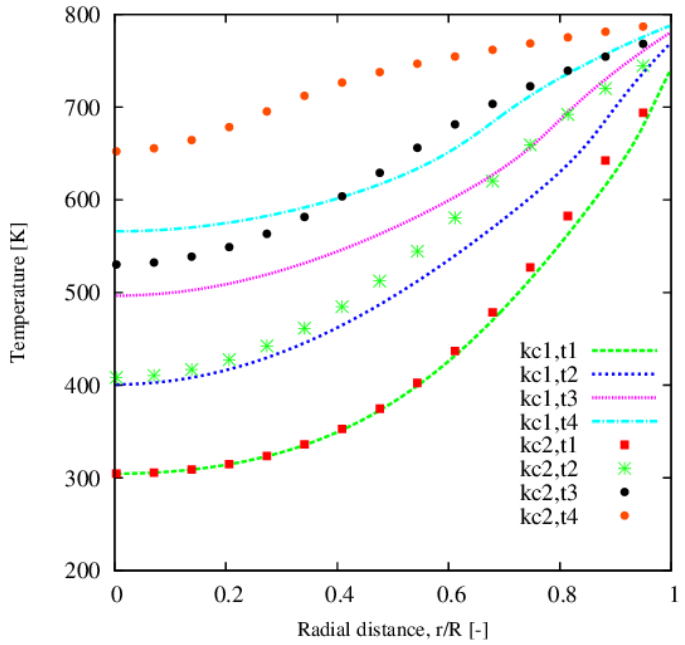

(a) Temperature profiles

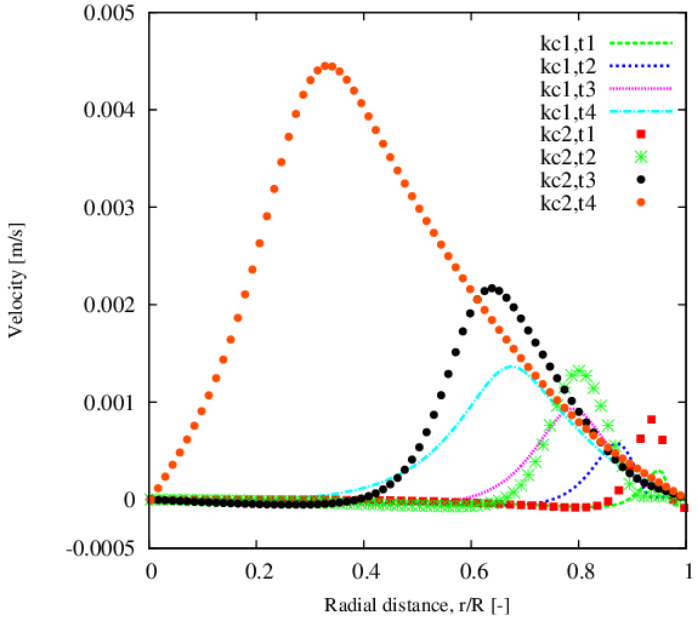

(b) Velocity profiles

Figure 8: Temperature and velocity profiles for several elapse times at two values of char thermal conductivity: kc1 = 3×10^{-2} W m^{-1} K^{-1}, kc2 = 15×10^{-2} W m^{-1} K^{-1} , t1 = 100 s, t2 = 200 s, t3 = 300 s, t4 = 400 s

5. Conclusions

Effects of thermo-physical properties on intra-particle secondary reactions during biomass pyrolysis have been investigated numerically. Parameters such as biomass thermal conductivity, density and char thermal conductivity

were used in this study. Wood cylinders (30 mm diameter) were used to represent thermally thick pyrolysis regime. As would be expected, biomass conversion time increased as biomass density increased. Increase in thermal conductivity however reduces biomass conversion time. Results also showed that velocity profiles and invariably, intra-particle volatile residence times are influenced by biomass thermo-physical properties. A combination of the rate of volatile production, intra-particle fluid flow velocity and spatial temperature distribution will dictate the eventual product yield distribution.

Nomenclature

A: pre-exponential factor	(1/s)
B: permeability	(m^2)
Cp: specific heat capacity	(J/ kg K)
Dpore: pore diameter	(m)
E: activation energy	(J/mol)
e: emissivity	(-)
h_c: convective heat transfer coefficient	(W/ m^2 K)
k: reaction rate constant	(1/s)
k_c: char thermal conductivity	(W/m K)
k_w: wood thermal conductivity	(W/m K)
M: molecular weight	(kg/mol)
P: Pressure	(Pa)
Q: heat generation	(W/m^3)
Q_c: convective heat flux	(W/m^2)
Q_r: radiation heat flux	(W/m^2)
R: universal gas constant	(J/mol K)
R: total radial length	(m)
r: radial axis	(m)
S: source term	
T: temperature	(K)
t : time	(s)
V: velocity	(m/s)
V_c: control volume	(m^3)
ε: porosity	(-)
ε_0: initial porosity	(-)
Δh: heat of reaction	(kJ/kg)
μ: viscosity	(kg/m s)
ρ: density	(kg/m^3)
$\rho_{w,0}$: initial density of wood	(kg/m^3)
σ: Stefan-Boltzmann constant	(W/m^2 K^4)
η: degree of pyrolysis	(W/m^2 K^4)

Subscripts
Ar: Argon
c: char, primary char formation reaction
c_2: secondary char formation reaction
g: gas, primary gas formation reaction
g_2: secondary gas formation reaction
is: intermediate solid, intermediate solid formation reaction
t: tar, tar formation reaction
v: total volatile
w: wood

References

[1] GrØnli, M.G. and Melaaen, M.C. (1999). Mathematical Model for Wood Pyrolysis-Comparison of

Experimental Measurements with Model Predictions. *Energy & Fuel* **14**, 791-800.
[2] Li, X.T., Grace, J.R., Lim, C.J., Watkinson, A.P., Chen, H.P. & Kim, J.R. (2004). Biomass Gasification in a Circulating Fluidized Bed. *Biomass and Bioenergy* **26**(2), 171-193
[3] Han, J. & Kim, H. (2008). The Reduction and Control Technology of Tar during Biomass Gasification/Pyrolysis: An Overview. *Renewable and Sustainable Energy Reviews* **12**, 397-416.
[4] Fagbemi, L., Khezami, L. & Capart, R. (2001). Pyrolysis Products from Different Biomasses: Application to the Thermal Cracking of Tar. *Applied Energy* **69,** 293-306.
[5] Antal, M.J. (1985). Effects of Reactor Severity on the gas-phase Pyrolysis of Cellulose and Craft Lignin-derived Volatile Matter. *Industrial & Engineering Chemistry Product Research and Development* **22**(2), 366-375. In: Di Blasi C. (2008). Modeling chemical and physical processes of wood and biomass pyrolysis. Progress in Energy and Combustion Science 34, 47-90
[6] Houben, M.P., De Lange, H.C. & Van Steenhoven A.A. (2005). Tar Reduction through Partial Combustion of Fuel Gas. *Fuel* **84**, 817-824.
[7] Hanaoka, T., Inoue, S., Uno, S., Ogi, T., Minowa, T. (2005) Effect of Woody Biomass Components on Air-stream Gasification. *Biomass and Bioenergy* **28**, 69-76.
[8] Lv, P.M., Xiong, Z.H., Chang, J., Wu, C.Z. & Chen, Y. (2004). An Experimental Study on Biomass Air-stream Gasification in aFluidized Bed. *Bioresource Technology* **95**, 95-101.
[9] Zainal, Z.A., Rifau, A., Ouadir, G.A. & Seetharamu K.N. (2002). Experimantal Investigation of a Downdraft Biomass Gasifier. *Biomass and Bioenergy* **23**, 283-289.
[10] Garcia-Ibanez, P., Cabanillas, A., Sanchez, J.M. (2004). Gasification of Leached Orujillo (Oil Olive Waste) in a Pilot Plant Circulating Fluidised Bed Reactor. Preliminary Results. *Biomass and Bioenergy* **27**, 183-194.
[11] Li, S., Xu, S., Liu, S., Yang, C. and Lu, Q. (2004). Fast Pyrolysis of Biomass in Free-fall Reactor for Hydrogen-rich Gas. *Fuel Process and Technology* **85**, 1201-1211.
[12] Narvàez, I., Orio, A., Aznar, M.P. & Corella, J. (1996). Biomass Gasification with Air in an Atmospheric Bubbling Fluidiczed Bed. Effect of Six Operational Variables on the Quality of the Produced Raw Gas. *Industrial Engineering Chemistry Research*, **35**(7), 2110-2120.
[13] Okekunle, P.O., Pattanotai, T., Watanabe, H. & Okazaki, K. (2011). Numerical and Experimental Investigation of Intra-particle Heat Transfer and Tar Decomposition during Pyrolysis of Wood Biomass. *Journal of Thermal Science and Technology* **6**(3), 360-375.
[14] Kosstrin H. (1980). Direct Formation of Pyrolysis Oil from Biomass. In: Proceedings, Specialists Workshop on Fast Pyrolysis of Biomass. In: Han, J. & Kim, H. (2008). The Reduction and Control Technology of Tar during Biomass Gasification/Pyrolysis: An Overview. *Renewable and Sustainable Energy Reviews* **12**, 397-416.
[15] Knight, R.A. (2000). Experience with Raw Gas Analysis from Pressurized Gasification of Biomass. *Biomass and Bioenergy* **18**, 67-77.
[16] Okekunle, P.O., Watanabe, H., Pattanotai, T. & Okazaki, K. (2012). Effect of biomass Size and Aspect Ratio on Intra-particle Tar Decomposition during Wood Cylinder Pyrolysis. *Journal of Thermal Science and Technology*, **7**(1), 1-15
[17] Okekunle, P.O., Watanabe, H. & Okazaki, K. (2013). Analysis of Biomass Pyrolysis Product Yield Distribution in Thermally Thin Regime at Different Heating Rates. *Mathematical Theory and Modeling* **3**(11), 28-34.
[18] Park, W.C., Atreya, A. & Baum, H.R. (2010). Experimental and Theoretical Investigation of Heat and Mass Transfer Processes during Wood Pyrolysis. *Combustion and Flame* **157,** 481-494.
[19] Di Blasi, C. (1996). Heat, Momentum and Mass Transport through a shrinking biomass Particle Exposed to Thermal Radiation. *Chemical Engineering science,* **51**(7), 1121-1132
[20] Chan, W.R.C., Kelbon, M. and Krieger, B.B. (1985). Modeling and Experimental verification of physical and Chemical Processes during Pyrolysis of a Large Biomass Particle. *Fuel* **64**, 1505-1513.
[21] Di Blasi, C. (1996). Influence of Physical Properties on Biomass Devolatilization Characteristics. *Fuel* **76**(10), 957-964.
[22] Jarvinen, M.P., Zevenhoven, R. & Vakkilainen, E.K. (2002). Auto-gasification of a Biofuel. *Combustion and Flame* **131**, 357-370.
[23] Babu, B.V. & Chaurasia, A.S. (2003). Modeling for Pyrolysis of Solid Particle: Kinetics and Heat Transfer Effects. *Energy Conversion and Management* **44**, 2251-2275
[24] Pyle, D.L. & Zaror, C.A. (1984). Heat transfer and kinetics in the low temperature pyrolysis of solids. *Chemical Engineering Science* **39**(1), 147-158.